G-protein–coupled receptor GPR161 is overexpressed in breast cancer and is a promoter of cell proliferation and invasion

Michael E. Feigin[a,1], Bin Xue[a,b], Molly C. Hammell[a], and Senthil K. Muthuswamy[a,b,c,1]

[a]Cold Spring Harbor Laboratory, Cold Spring Harbor, NY 11724; [b]Department of Molecular and Cellular Biology, Stony Brook University, Stony Brook, NY 11794; and [c]Department of Medical Biophysics, Princess Margaret Cancer Center, Campbell Family Institute for Breast Cancer Research, University of Toronto, Toronto, ON, Canada M5G 1L7

Edited by Tak W. Mak, The Campbell Family Institute for Breast Cancer Research at Princess Margaret Cancer Centre, Ontario Cancer Institute, University Health Network, Toronto, Canada, and approved February 11, 2014 (received for review October 28, 2013)

Triple-negative breast cancer (TNBC) accounts for 20% of breast cancer in women and lacks an effective targeted therapy. Therefore, finding common vulnerabilities in these tumors represents an opportunity for more effective treatment. Despite the growing appreciation of G-protein–coupled receptor (GPCR)-mediated signaling in cancer pathogenesis, very little is known about the role GPCRs play in TNBC. Using genomic information of human breast cancer, we have discovered that the orphan GPCR, G-protein–coupled receptor 161 (*GPR161*) is overexpressed specifically in TNBC and correlates with poor prognosis. Knockdown of *GPR161* impairs proliferation of human basal breast cancer cell lines. Overexpression of *GPR161* in human mammary epithelial cells increases cell proliferation, migration, intracellular accumulation of E-cadherin, and formation of multiacinar structures in 3D culture. GPR161 forms a signaling complex with the scaffold proteins β-arrestin 2 and Ile Gln motif containing GTPase Activating Protein 1, a regulator of mammalian target of rapamycin complex 1 and E-cadherin. Consistently, *GPR161* amplified breast tumors and cells overexpressing *GPR161* activate mammalian target of rapamycin signaling and decrease Ile Gln motif containing GTPase Activating Protein 1 phosphorylation. Thus, we identify the orphan GPCR, GPR161, as an important regulator and a potential drug target for TNBC.

G-protein–coupled receptors (GPCRs) are heptahelical membrane proteins responsible for transducing signals from a diverse range of ligands to affect numerous physiological processes, including vision, olfaction, behavior, and autonomic nervous system transmission (1). These properties have allowed the widespread development of GPCR-targeted drugs, which represent nearly 30% of all currently used therapeutics, for indications ranging from allergy to depression to hypertension. However, the clinical utility of targeting GPCRs in cancer therapy remains poorly defined (2, 3). GPCRs regulate many aspects of tumorigenesis, including proliferation, invasion, survival at the secondary site, and immune cell function, as well as several cancer-associated signaling pathways (4). Emerging large-scale genomic analyses have recently provided further evidence of frequent GPCR alterations in human tumors (5–10). For example, 20% of all human tumors sequenced contain mutations in GPCRs; the phenotypic outcome of these mutations remains unknown and thus provides a wealth of information for the development of hypothesis-driven experiments (5). In addition to mutations, alterations in gene expression, copy number, and promoter methylation of GPCRs have been detected. Determining the contribution of such alterations to cancer initiation and progression remains a significant challenge yet critical both for discovery of driver oncogenes and for the development of targeted therapeutics.

Triple-negative breast cancer (TNBC), characterized by lack of expression of estrogen receptor (ER), progesterone receptor (PR), and epidermal growth factor receptor 2 (*HER2*), is associated with early recurrence and poor outcome (11). Mutations in *BRCA1* and *BRCA2* account for 15% of TNBC, and several other susceptibility loci have been identified (12). Representing nearly a quarter of all breast cancers, TNBC lacks an effective targeted therapy due to high levels of genetic heterogeneity. Therefore, finding common druggable targets is a critical endeavor. We used large-scale genomic analysis to discover GPCRs up-regulated in TNBC. This method uncovered the poorly characterized class A rhodopsin family orphan GPCR, GPR161.

Several studies have identified an important role for GPR161 during normal development. An 8 bp mutation in *GPR161*, resulting in a premature stop codon and truncated C terminus, was identified as the cause of the vacuolated lens spontaneous mouse model, exhibiting neural tube defects and congenital cataracts (13). Consistent with these phenotypes, GPR161 is expressed in the lateral neural folds and in the developing lens (13). Knockdown of *GPR161* in the zebrafish embryo disrupts left–right patterning in the lateral plate mesoderm through modulation of Ca^{2+} levels, resulting in aberrant cardiac morphogenesis (14). Recently, GPR161 was shown to localize to primary cilia and regulate Sonic hedgehog (Shh) signaling (15). Expression of *GPR161* inhibits Shh through Gαs-induced cyclic adenosine monophosphate (cAMP) accumulation, resulting in protein kinase A–mediated processing of Gli3 (15). In addition, GPR161 is part of a signaling network that confers resistance to MAP kinase pathway inhibition in melanoma (16).

We describe a role for GPR161 in the pathogenesis of human TNBC. We provide evidence that GPR161 promotes proliferation through activation of mammalian target of rapamycin

Significance

Recent advances in DNA sequencing and bioinformatics tools have allowed the large-scale characterization of genetic alterations in human tumors. We exploited genomics data to identify commonly occurring alterations in G-protein–coupled receptors (GPCRs) in triple-negative breast cancer (TNBC), a subset of breast cancer with poor prognosis and lacking effective targeted therapy. We have discovered that the orphan GPCR, G-protein–coupled receptor 161 (*GPR161*), is overexpressed specifically in TNBC and correlates with poor prognosis. We identify GPR161 as a regulator of mammary epithelial cell proliferation and invasion in a mammalian target of rapamycin signaling-pathway–dependent manner. Down-regulation of GPR161 in a TNBC-derived cell line impairs cell growth, suggesting that GPR161 is a drug target for breast cancer.

Author contributions: M.E.F. and S.K.M. designed research; M.E.F. and M.C.H. performed research; B.X. contributed new reagents/analytic tools; M.E.F., M.C.H., and S.K.M. analyzed data; and M.E.F. and S.K.M. wrote the paper.

The authors declare no conflict of interest.

This article is a PNAS Direct Submission.

[1]To whom correspondence may be addressed. E-mail: s.muthuswamy@utoronto.ca or feiginm@cshl.edu.

This article contains supporting information online at www.pnas.org/lookup/suppl/doi:10.1073/pnas.1320239111/-/DCSupplemental.

complex 1 (mTORC1), stimulates migration and invasion, and disrupts E-cadherin (E-cad) localization. We also identify a protein complex consisting of GPR161 and the scaffold proteins β-arrestin 2 (βArr2) and IQ motif containing GTPase Activating Protein 1 (IQGAP1), and demonstrate that GPR161 induces proliferation and migration in an IQGAP1-dependent manner. We identify *GPR161* as a promoter of cancer cell proliferation and migration and as a promising drug target in TNBC.

Results

GPR161 Is Overexpressed in TNBC. The lack of common genetic alterations in TNBC has hampered the development of targeted therapies. To identify potential targets, we used the large-scale analyses of patient tumor samples from The Cancer Genome Atlas (TCGA) to identify GPCR specifically up-regulated in TNBC. GPCRs were selected for this analysis for their amenability to inhibition by small molecules, peptides, and antibodies and their regulation of several cancer-associated signaling pathways. We determined the reads per kilobase per million reads (RPKM) of 366 nonsensory GPCRs from RNAseq data generated by TCGA. Forty-five GPCRs were significantly overexpressed (greater than twofold) in TNBC compared with unmatched normal breast tissue. We chose to first investigate the biological function of *GPR161* due to the limited current knowledge about its role in cancer. We found that *GPR161* was up-regulated 2.2-fold in TNBC versus unmatched normal breast tissue (Fig. 1*A*). We extended this analysis to other breast cancer subtypes, including the ER-positive Luminal A and B (LumA/B), as well as HER2-positive tumors (Fig. 1*A*). Although there was no change in *GPR161* expression in HER2-positive tumors, *GPR161* expression decreased significantly in LumA (0.683-fold change from control, $P < 1 \times 10^{-10}$) and LumB (0.781-fold change from control, $P < 2.22 \times 10^{-5}$). This correlation was consistent in the Richardson Breast 2 panel, with *GPR161* showing a 2.1-fold increase in ductal breast cancer compared with normal breast (Fig. S1*A*), and the Farmer Breast study, with *GPR161* showing a 2.3-fold increase in basal-like invasive breast cancer (IBC) versus luminal-like IBC (Fig. S1*B*). Therefore, *GPR161* was specifically overexpressed in human TNBC.

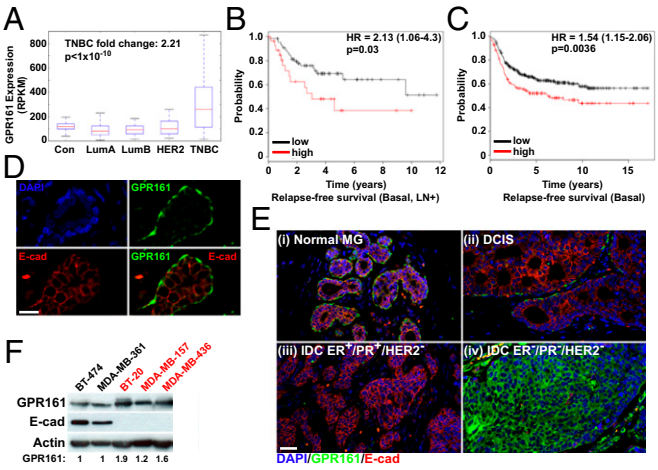

Fig. 1. GPR161 is overexpressed in TNBC. (*A*) GPR161 expression was analyzed in 530 LumA, 88 LumB, 32 HER2, 98 TNBC, and 100 nonmatched controls. *P* values were calculated with a Mann–Whitney *U* test. (*B*) Kaplan–Meier analysis of effect of GPR161 expression on relapse-free survival in basal, lymph-node–positive breast cancer patients. *P* values were calculated with a Log Rank Test. (*C*) Kaplan–Meier analysis of effect of GPR161 expression on relapse-free survival in basal breast cancer patients. *P* values were calculated with a log rank test. (*D*) Immunohistochemical (IHC) analysis of GPR161 and E-cad in normal human mammary gland. (Scale bar, 10 μm.) (*E*) IHC analysis of GPR161 and E-cad in normal human mammary gland (*i*), DCIS (*ii*), and IDC, either ER^+/PR^+ (*iii*) or triple-negative (*iv*). (Scale bar, 30 μm.) (*F*) Expression of GPR161 was measured by Western blot in luminal (BT-474 and MDA-MB-361) and TNBC (BT-20, MDA-MB-157, and MDA-MB-436) cell lines.

High Expression of GPR161 Correlates with Relapse in Human TNBC. To determine the clinical relevance of *GPR161* expression, we compared relapse-free survival rates for breast cancer patients within the highest or lowest quartiles of *GPR161* expression (Fig. S1*C* and Fig. 1 *B* and *C*). Among basal breast cancer patients with lymph-node–positive disease, high *GPR161* expression decreased time to relapse by 113% (hazard ratio, HR = 2.13) (Fig. 1*B*). Time to relapse decreased 54% when all basal breast cancers were analyzed (HR = 1.54) (Fig. 1*C*). Finally, for patients with any type of breast cancer, high *GPR161* expression was correlated with a 27% decrease in time to relapse (HR = 1.27) (Fig. S1*C*). Therefore, *GPR161* was overexpressed in basal breast cancer and had prognostic value.

GPR161 Is Expressed in Basal/Myoepithelial Cells in Normal and Cancer Cells. To determine the normal expression pattern of GPR161 in the human mammary gland, we costained breast tissue with antibodies specific for GPR161 and the luminal epithelial marker E-cad (Fig. 1 *D* and *E*, *i*). GPR161 expression was detected solely in the myoepithelium, and not in the E-cad–positive luminal epithelial cells that surround the luminal space. To extend our gene expression analysis of GPR161 in breast cancer to the protein level, we performed immunohistochemical analysis of GPR161 and E-cad in a human breast cancer tissue array. In early stage disease (ductal carcinoma in situ, DCIS), there was no change detected in the GPR161-positive population, whereas the E-cad–positive population increased in number (Fig. 1 *E*, *ii*). Among the 20 ER+ invasive ductal carcinoma (IDC) tumors analyzed, 19 showed strong E-cad staining, with only one staining positive for GPR161 (Fig. 1 *E*, *iii*). In contrast, four out of six triple-negative IDC tumor samples stained strongly for GPR161 (Fig. 1 *E*, *iv*). Consistent with these observations, GPR161 protein levels were higher in three triple-negative cell lines (BT-20, MDA-MB-157, and MDA-MB-436) than two luminal-like cell lines (BT-474 and MDA-MB-361) (Fig. 1*F*). Taken together, these results demonstrate that GPR161 was overexpressed in human TNBC and TNBC cell lines.

GPR161 Induces Multiacinar Formation in 3D Culture. To begin to understand the biological relevance of GPR161 overexpression, we generated MCF-10A cells overexpressing GPR161 (Fig. 2*A*). Stable populations were selected after infection with GPR161 retrovirus and analyzed for GPR161 expression (Fig. 2*A*). We chose lines with modest GPR161 overexpression, in accordance with the 2.2-fold increase noted in human tumor samples (Fig. 1*A*). When grown on a 3D Matrigel layer, MCF-10A cells form acinar structures with hollow lumens (17). Activation of oncogenes in this context disrupts acinar morphogenesis and can result in large, disorganized multiacinar structures (17). To probe the impact of GPR161 overexpression on acinar morphogenesis, we grew MCF-10A cells [either murine stem cell virus-puromycin-IRES-GFP (MSCV-PIG) or GPR161] in 3D culture for 14 d (Fig. 2*B*). Whereas control acini formed round, regular structures, cells expressing GPR161 formed large, multiacinar structures (Fig. 2 *B* and *C*). Overexpression of GPR161 in MDA-MB-361 cells grown in 3D culture similarly disrupted 3D growth (Fig. S1 *D* and *E*). Optical sectioning through the center of the MCF-10A acini revealed the appearance of hollow lumens in control acini (Fig. 2*B*, *Lower Left* DAPI image). In contrast, GPR161-expressing MCF-10A acini displayed filled lumens (Fig. 2*B*, *Lower Right* DAPI image). Quantitative analysis of acinar size showed a greater than twofold increase in GPR161-expressing acini than controls (Fig. 2*C*). To determine the mechanism by which GPR161 induced multiacinar formation and filled lumens, we analyzed proliferation in day 14 acini (Fig. 2*D*). In control acini, proliferation was low and Ki67 was rarely detected in the lumen (6.3% of acini). In contrast, in GPR161 acini, proliferation was maintained at day 14 and Ki67+ cells were detected in the lumens of 57.5% of the acini

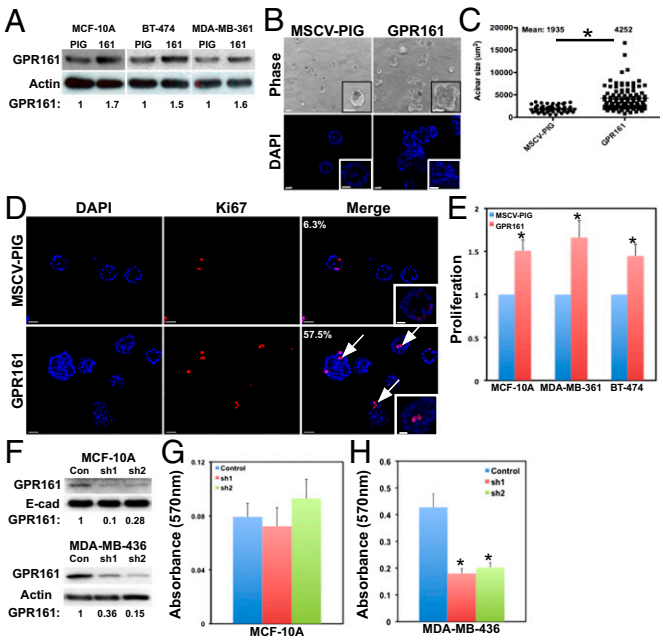

Fig. 2. GPR161 overexpression induces cell proliferation. (*A*) Western blot analysis of GPR161 overexpression in MCF-10A, BT-474, and MDA-MB-361 cells. (*B*) MCF-10A cells, either MSCV-PIG or GPR161, were grown as 3D acini for 14 d. Phase contrast (upper panels) and DAPI staining (lower panels) were used to monitor acinar morphology. [Scale bar, 100 μm (*Upper*), 75 μm (*Upper Inset*), 50 μm (*Lower*), and 20 μm (*Lower Inset*).] (*C*) Acinar area was measured for MSCV-PIG and GPR161 MCF-10A acini. $*P < 0.05$ for the difference between GPR161 cells and those expressing the empty vector using an unpaired *t* test. (*D*) Proliferation was analyzed in MCF-10A acini by IF staining of Ki67. Arrows denote Ki67-positive central acinar cells. [Scale bar, 50 μm and (*Inset*) 20 μm.] (*E*) MTT assay was used to measure cell proliferation in the nontransformed mammary epithelial cell line MCF-10A and the luminal cancer cell lines MDA-MB-361 and BT-474, stably expressing an empty vector (MSCV-PIG) or GPR161. $*P < 0.05$ for the difference between GPR161 cells and those expressing the empty vector using an unpaired *t* test. (*F*) Western blot analysis of GPR161 knockdown in MCF-10A and MDA-MB-436 cells. (*G*) MTT assay was used to measure cell proliferation in control or GPR161-deficient MCF-10A cells. (*H*) MTT assay was used to measure cell proliferation in control or GPR161-deficient MDA-MB-436 cells. $*P < 0.05$ for the difference between cells expressing a control shRNA and those with a GPR161 shRNA using an unpaired *t* test.

(see arrows in Fig. 2*D*). Therefore, overexpression of GPR161 induced cell proliferation and disrupted morphogenesis of mammary epithelial cells grown in 3D culture.

GPR161 Regulates Proliferation in Mammary Cell Lines. To rule out the possibility that GPR161-induced proliferation was restricted to basal epithelial cells, we also overexpressed (less that 2.0-fold) GPR161 in two luminal-like breast cancer cell lines (BT-474 and MDA-MB-361) (Fig. 2*A*). Overexpression of GPR161 increased proliferation of MCF-10A cells compared with cells expressing an empty vector (MSCV-PIG) (Fig. 2*E*). Similarly, GPR161 overexpression increased proliferation in both MDA-MB-361 and BT-474 cells (Fig. 2*E* and Fig. S1*F*). Therefore, overexpression of GPR161 to the levels seen in TNBC can enhance proliferation in mammary epithelial cells and cancer-derived luminal tumor cell lines.

To determine if GPR161 is required for proliferation of basal breast cancer cells, we used shRNA to knock down GPR161 in MCF-10A and MDA-MB-436 TNBC cell lines (Fig. 2*F*). Two hairpins significantly reduced GPR161 expression compared with a control shRNA in both cell lines. GPR161 knockdown had no significant effect on proliferation of nontransformed MCF-10A cells (Fig. 2*G*). However, proliferation was reduced more than twofold in MDA-MB-436 cells, likely because the cancer cells and not MCF-10A have developed a dependence on GPR161-regulated pathways (Fig. 2*H*). Therefore, GPR161 is both necessary and sufficient for regulating proliferation in breast cancer cells.

GPR161 Induces Cell Proliferation Through mTOR. To obtain insight into pathways activated in tumors with high levels of GPR161, we analyzed reverse phase protein array (RPPA) data from the TCGA database. Tumors with high levels of GPR161 had higher phosphorylation of mammalian target of rapamycin (mTOR) pathway components EIF4BP1, RPS6KA1, JUN, and RB1 compared with tumors expressing lower levels of GPR161 (Fig. 3*A*). We investigated if GPR161 overexpression activated the mTOR signaling pathway in cells in culture. Under normal growth conditions, control MDA-MD-361 cells display low levels of phosphorylation of the AKT pathway component p70S6 kinase (p70S6K) at T389 and the downstream target, ribosomal protein S6, at S235/236 (Fig. 3*B*). In contrast, cells expressing GPR161 display enhanced phospho-p70S6K and phospho-S6. A similar pattern of S6 phosphorylation is observed in control and GPR161-expressing BT-474 cells (Fig. S2*A*). mTOR activation is inhibited by PRAS40 and phosphorylation of PRAS40 at Thr246 relieves this inhibition (18). Therefore, we monitored PRAS40 phosphorylation in MDA-MD-361 cells expressing an empty vector or GPR161. Phospho-PRAS40 was markedly increased in GPR161-expressing cells (Fig. 3*B*). Similarly, we detected increased mTOR phosphorylation at S2448 in GPR161-expressing cells (Fig. 3*B*). To determine the relevance of mTOR activation in the GPR161-induced phosphorylation of S6, we treated the cells with rapamycin, an mTOR inhibitor (Fig. 3*C*). Although phospho-S6 levels were higher in GPR161-expressing cells, this increase was abolished upon rapamycin treatment. Therefore, GPR161-induced S6 phosphorylation was mTORC1-dependent. To determine the relevance of the mTOR pathway to GPR161-induced proliferation, MDA-MB-361 cell growth was measured in the absence and presence of rapamycin (Fig. 3*D*). GPR161-induced cell proliferation was inhibited in the presence of rapamycin. Furthermore, rapamycin treatment inhibited multiacinar structure formation in GPR161-expressing MCF-10A acini (Fig. 3 *E* and *F*). These observations suggest that GPR161 mediates cell proliferation in an mTORC1-dependent manner.

GPR161 Induces Migration and Invasion of Mammary Epithelial Cells. When grown on standard tissue culture dishes, GPR161-expressing cells displayed robust changes in cell shape. Subconfluent MCF-10A and MDA-MB-361 cells formed epithelial cell colonies with smooth, round edges (Fig. S2 *B* and *C*). In contrast, cells expressing GPR161 formed colonies with poorly defined colony borders, with sharp edges and protrusions (Fig. S2 *B* and *C*), suggesting migratory/invasive properties. Consistent with this possibility, overexpression of GPR161 led to a twofold increase in the migratory ability of MDA-MB-361 and BT-474 cells, as monitored by transwell migration assay over 24 h (Fig. 4*A*). Invasive potential was determined by culturing GPR161-expressing MCF-10A cells in 3D in a 1:1 mix of Matrigel and collagen. Whereas control cells formed round, noninvasive structures, GPR161-expressing MCF-10A acini were multiacinar and invasive (Fig. 4*B*). GPR161-expressing acini also had disrupted Laminin-V staining, a hallmark of invasion in MCF-10A culture (Fig. 4*C*).

GPR161 Induces Intracellular Accumulation of E-cad. The GPR161-induced change in cell shape and invasive ability led us to investigate the possibility that the cells had undergone an epithelial-to-mesenchymal transition. However, Western blot analysis of protein lysates from control and GPR161-expressing MCF-10A cells failed to show changes in the levels of the mesenchymal markers vimentin, snail, fibronectin, and *N*-cadherin (Fig. S2*D*).

Close inspection of the GPR161-expressing MCF-10A acinar structures revealed a rough surface topology, suggesting a defect in cell–cell adhesion (Fig. 4*D*). Therefore, we probed the localization of the adherens junction protein E-cad in GPR161-expressing

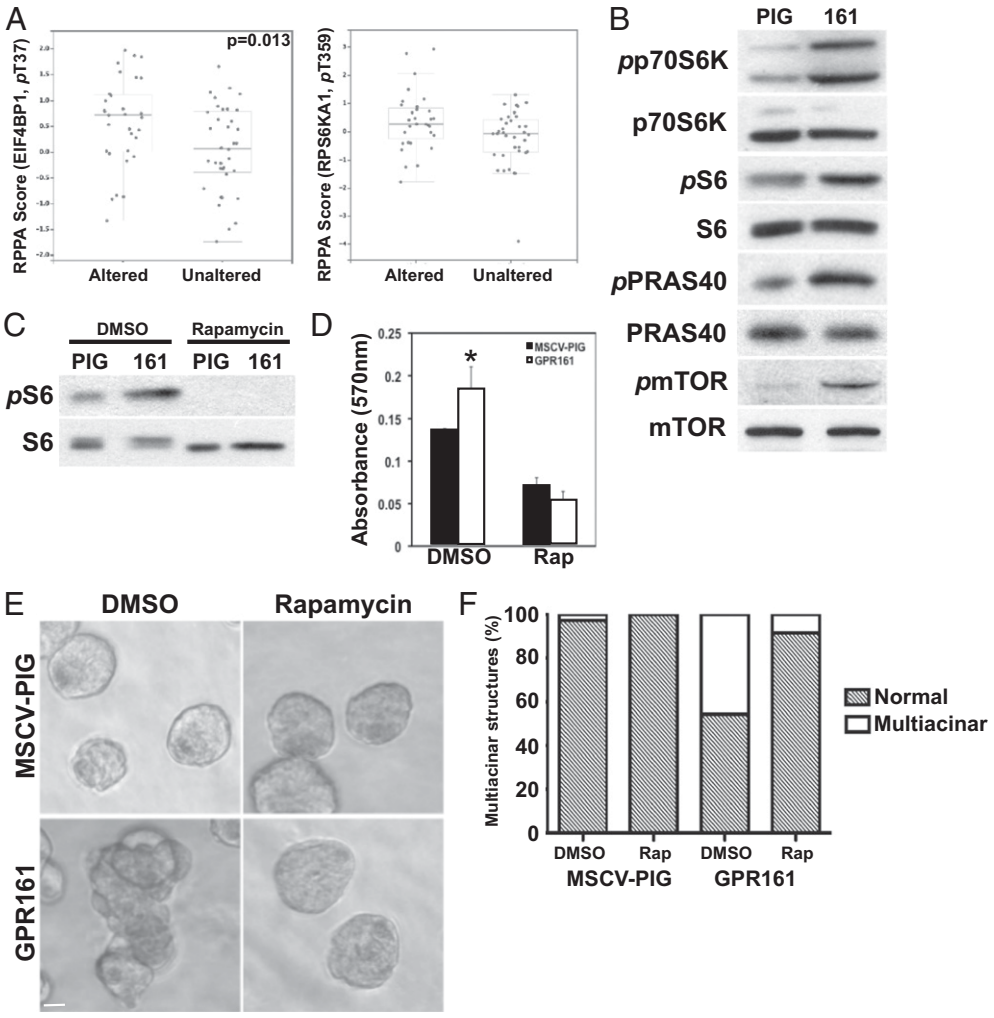

Fig. 3. GPR161 induces activation of mTORC1. (*A*) Analysis of RPPA data generated from TCGA among basal breast cancer samples, comparing those with or without alterations in GPR161. A two-sided two-sample *t* test was used to calculate *P* values. (*B*) Western blot analysis of cell lysates from MDA-MB-361 MSCV-PIG and GPR161 cells was used to detect phosphorylation of PI3K pathway components. (*C*) MDA-MB-361 MSCV-PIG and GPR161 cells were pretreated with 20 nM rapamycin for 30 min before cell lysis. Phosphorylation of S6 was detected by Western blot. (*D*) MTT assay was used to measure cell proliferation in MDA-MB-361 cells either stably expressing an empty vector (MSCV-PIG) or GPR161. Cells were treated with DMSO or 20 nM rapamycin. $*P < 0.05$ using an unpaired *t* test. (*E*) MCF-10A cells, either MSCV-PIG or GPR161, were grown as 3D acini for 14 d in the presence or absence of 20 nM rapamycin. Acinar morphology was analyzed by phase contrast microscopy. (Scale bar, 20 μm.) (*F*) Quantification of multiacinar structure formation from *E*.

cells. Total levels of E-cad were modestly reduced upon expression of GPR161. In addition, GPR161-expressing MCF-10A cells displayed markedly higher levels of intracellular E-cad than control cells as measured by immunoblot (Fig. 4*E*). This pattern was similar in MDA-MB-361 cells, where E-cad was localized to the cytosol upon GPR161 expression as detected by immunofluorescence (Fig. 4*F*). This observation was extended to human tumors, where four TNBC samples expressing high levels of GPR161 displayed intracellular E-cad, compared with predominantly plasma-membrane–localized E-cad in six ER+/GPR161– tumors (Fig. 4*G* and Fig. S2*E*). Therefore, GPR161 expression is associated with both decrease in levels and redistribution of E-cad from the plasma membrane in epithelial cells.

GPR161 Forms a Complex with IQGAP1 and βArr2. To define the mechanism by which GPR161 induces proliferation, migration, and invasion, we focused on an adherens junction-localized scaffold protein that is related to GPCR signaling. IQGAP1 regulates a vast array of cellular functions through interactions with proteins such as E-cad, Neural Wiskott-Aldrich syndrome protein (N-WASP), Cdc42, and the exocyst complex (19). IQGAP1 has been reported to interact with βArr2, a scaffold protein that binds to activated GPCRs and regulates signaling and receptor endocytosis (20). IQGAP1 promotes proliferation and migration, and overexpression has been associated with poor prog-nosis in advanced colorectal cancer (21–23). Interestingly, IQGAP1 can coordinate cell growth and division in a phosphorylation-dependent manner (24). Phosphorylation of IQGAP1 at Ser1339 by protein kinase C allows binding of Cdc42 (25), whereas unphosphorylated IQGAP1 binds mTOR and leads to activation of downstream signals, including phosphorylation of S6 (26, 27). To determine if GPR161 overexpression influences the phosphorylation status of IQGAP1, we immunoprecipitated endogenous IQGAP1 from control or GPR161-expressing MCF-10A and MDA-MB-361 cells and analyzed serine phosphorylation by immunoblot analysis (Fig. 5*A*). In both cell lines, expression of GPR161 induced a striking decrease in IQGAP1 serine phosphorylation, consistent with GPR161-induced mTOR activation.

To test the possibility that GPR161 forms a signaling complex with IQGAP1 and βArr2, we immunoprecipated myc-tagged IQGAP1 from 293T cell lysates coexpressing FLAG-tagged GPR161 (Fig. 5*B*). Myc-IQGAP1 was able to pull down FLAG-GPR161. Immunoprecipitation (IP) of βArr1 failed to pull down either myc-IQGAP1 or FLAG-GPR161 (Fig. 5*C*, center lane). In contrast, IP of βArr2 pulled down both myc-IQGAP1 and FLAG-GPR161 (Fig. 5*C*, right lane) in cells coexpressing FLAG-GPR161, myc-IQGAP1 with either HA-tagged βArr1 or βArr2. Furthermore, IP of endogenous GPR161 immunoprecipitated both IQGAP1 and βArr2, and IQGAP1 immunoprecipitated GPR161 and βArr2 (Fig. 5*D*). Although these results do not prove the existence of a trimeric complex, they suggest that βArr2 may serve as a scaffold connecting GPR161 and IQGAP1.

To determine the requirement for IQGAP1 in GPR161-induced proliferation and migration, we used siRNA to knock down IQGAP1 in MDA-MB-361 cells (Fig. 5*E*). Knockdown of IQGAP1 attenuated both GPR161-induced proliferation (Fig. 5*F*)

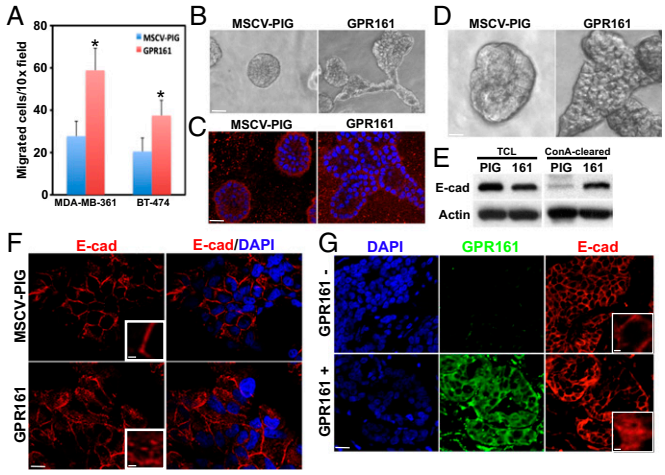

Fig. 4. GPR161 induces migration and invasion of mammary epithelial cells. (*A*) Quantification of transwell migration assay of MDA-MB-361 and BT-474 cells either stably expressing an empty vector (MSCV-PIG) or GPR161. $*P < 0.05$ using an unpaired *t* test. (*B*) MCF-10A cells, either MSCV-PIG or GPR161, were grown as 3D acini in 1:1 Matrigel/collagen for 14 d. Phase contrast was used to monitor acinar morphology. (Scale bar, 20 μm.) (*C*) Invasion was analyzed in MCF-10A acini by IF staining of Laminin V. (Scale bar, 20 μm.) (*D*) MCF-10A cells, either MSCV-PIG or GPR161, were grown as 3D acini in 1:1 Matrigel/collagen for 14 d. Phase contrast was used to monitor acinar morphology. (Scale bar, 10 μm.) (*E*) Western blot analysis was used to measure E-cad levels from total MCF-10A cell lysates (TCLs) or those treated with Con A. (*F*) IF analysis of E-cad localization in MDA-MB-361 cells, either stably expressing an empty vector (MSCV-PIG) or GPR161. [Scale bar, 10 μm and (*Inset*) 20 μm.] (*G*) IF analysis of E-cad localization in human tumors expressing low or high levels of GPR161. [Scale bar, 20 μm and (*Inset*) 10 μm.]

and transwell migration (Fig. 5*G*). Therefore, GPR161 promotes cell proliferation and cell migrations in an IQGAP1-dependent manner.

GPR161 and IQGAP1 Are Coamplified in Human Breast Cancer. As both *GPR161* (this study) and *IQGAP1* (28) have been implicated in human breast cancer pathogenesis, we sought to investigate the cooccurrence of alterations in these two genes. Of the 748 tumors analyzed from the TCGA, 166 (22.2%) contained amplification of *GPR161* and 39 (5.2%) contained amplification of *IQGAP1* (Fig. 5*H*). Thirteen tumors contained alterations in both genes, a statistically significant outcome ($P < 0.036$) compared with that expected from random overlap. Despite the significant association observed in all breast cancers, TNBC represented a small subset and hence did not reach statistical significance. Therefore, there is likely a selection for coamplification of *GPR161* and *IQGAP1* during breast cancer progression.

Discussion

Taken together, our results identify *GPR161* as a prognostic biomarker for TNBC and demonstrate that GPR161 is an important regulator of cell proliferation and migration in breast cancer cells. We identify activation of mTORC1/S6K as an effector pathway and identify IQGAP1 and βArr2 as GPR161 binding partners. In addition, we uncover genetic interactions between *GPR161* and *IQGAP1* in human breast cancer.

Phosphorylation of the scaffold protein IQGAP1 has recently been recognized as a regulator of nutrient and growth factor signaling (24). Phosphorylation of IQGAP1 at Ser1443 allows binding of CDC42, whereas unphosphorylated IQGAP1 promotes activation of mTOR. We find that overexpression of GPR161 decreases IQGAP1 serine phosphorylation, consistent with the observed activation of mTORC1. Whether GPR161 reduces the activity of PKC (the IQGAP1 Ser1443 kinase), or activates an unknown phosphatase, remains to be determined.

Genomic analyses of human tumors have uncovered widespread alterations in GPCRs in numerous cancer types (5, 29). However, the contribution of these alterations to human tumorigenesis remains unknown. Our study used genomic information to identify *GPR161* as a regulator of mammary epithelial cell proliferation and invasion, and a putative drug target, in TNBC. We also identified two breast cancer *GPR161* mutations in the Catalog of Somatic Mutations in Cancer database. One mutation (R91G) is found within the first extracellular loop and may therefore play a role in ligand binding. The other, S251G, is within the third intracellular loop, a region known to be phosphorylated in response to activation of many GPCRs and the site of interaction of β-arrestins. The importance of these mutations in cancer remains to be investigated. However, we demonstrate that expression of *GPR161* is prognostic, suggesting a role for *GPR161* in determining patient outcomes. Interestingly, TCGA data across multiple cancer types uncover recurrent amplifications of *GPR161* in bladder urothelial carcinoma, lung adenocarcinoma, and melanoma. It is likely that developing ways to target *GPR161* may have implications beyond breast cancer.

Materials and Methods

Plasmids and Antibodies. The GPR161 cDNA was obtained from Origene and cloned into the MSCV-PIG retroviral vector. Expression vectors containing myc-IQGAP1, HA-βArr1, and HA-βArr2 were obtained from Addgene. Antibodies were obtained from the following sources: GPR161 (Abcam), E-cad (BD Biosciences), Actin (Sigma), Ki67 (Invitrogen), phospho-p70S6K (Cell Signaling), p70S6K (Cell Signaling), phospho-S6 (Cell Signaling), S6 (Cell Signaling), phospho-mTOR (Cell Signaling), mTOR (Cell Signaling), Laminin V

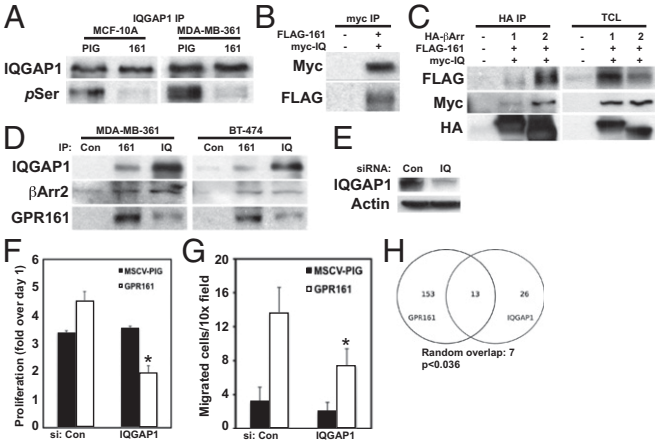

Fig. 5. GPR161 forms a protein complex with IQGAP1 and βArr2. (*A*) Western blot analysis of IQGAP1 serine phosphorylation in MCF-10A and MDA-MB-361 cells either stably expressing an empty vector (MSCV-PIG) or GPR161. (*B*) Myc-IQGAP1 and GPR161-FLAG were transfected into 293T cells, followed 48 h later by Myc-IP. Western blot analysis was used to detect Myc and FLAG. (*C*) Myc-IQGAP1, GPR161-FLAG, HA-βArr1, and HA-βArr2 were transfected into 293T cells, followed 48 h later by HA-IP. Western blot analysis was used to detect Myc, FLAG, and HA. (*D*) GPR161 and IQGAP1 antibodies were conjugated to protein G–Sepharose beads, followed by incubation with MDA-MB-361 and BT-474 cell lysates. Western blot analysis was used to detect co-IP of endogenous IQGAP1, βArr2, and GPR161. (*E*) Western blot analysis was used to detect knockdown of IQGAP1 in MDA-MB-361 cells. (*F*) MTT assay was used to measure cell proliferation in MDA-MB-361 cells (MSCV-PIG or GPR161) transfected with control or IQGAP1 siRNA. $*P < 0.05$ for the difference between GPR161-expressing cells treated with control or IQGAP1 siRNA using an unpaired *t* test. (*G*) Quantification of transwell migration assay of MDA-MB-361 cells either stably expressing an empty vector (MSCV-PIG) or GPR161 and transfected with control or IQGAP1 siRNA. $*P < 0.05$ for the difference between GPR161-expressing cells treated with control or IQGAP1 siRNA using an unpaired *t* test. (*H*) Expression of GPR161 and IQGAP1 was analyzed in 748 breast tumor samples. *P* values were calculated with Fisher's exact test.

(Millipore), IQGAP1 (Santa Cruz), phospho-Serine (Abcam), HA (Covance), myc (Cell Signaling), and Flag (Sigma).

Cell Culture and Transfection. Cells were cultured in the following medium: MCF-10A [DMEM/F12, 5% (vol/vol) horse serum, epidermal growth factor (20 ng/mL), hydrocortisone (0.5 μg/mL), cholera toxin (100 ng/mL), insulin (10 μg/mL), penicillin/streptomycin (P/S)], BT-474 [Improved Minimal Essential Medium, 10% FBS, Insulin (10 μg/mL), P/S], MDA-MB-361 [DMEM, 15% FBS, L-Glutamine (5 mL), nonessential amino acids (5 mL), P/S], BT-20 [DMEM, 15% (vol/vol) FBS, P/S], MDA-MB-157 (DMEM, 10% FBS, P/S), MDA-MB-436 (DMEM, 10% FBS, P/S), and 293T (DMEM, 10% FBS, P/S). Cells were transfected by using Lipofectamine 2000 (Invitrogen) according to the manufacturer's suggested protocol. Retroviruses expressing MSCV-PIG and GPR161 were prepared as described (30). GPR161 and control shRNA were ordered from Thermo Scientific. The GPR161 sequences are as follows: TCTTGTACAAGGTGACCAC and AGGACTTCTTGTACAAGGT. MCF-10A cells were cultured in 3D as previously described (17). Control and IQGAP1 siRNA were obtained from Sigma.

Cytosolic E-cad Assay. Samples were treated with Con A covalently linked to Sepharose (Amersham). Confluent cells were washed with PBS and lysed in radioimmunoprecipitation assay buffer (20 mM Tris·HCl, pH 7.4, 150 mM NaCl, 5 mM EDTA, 1% Triton X-100) plus aprotinin, leupeptin, and sodium orthovanadate. Lysates were rotated at 4 °C for 20 min and then centrifuged for 20 min at 20,000 × *g*. A total of 1.25 mg of each sample was diluted in 500 μL RIPA buffer. A total of 50 μL of Con A–Sepharose was added to each tube, which then were incubated at 4 °C for 1 h with rotation. After a brief centrifugation, the supernatant was removed to a fresh microfuge tube, 25 mL of Con A–Sepharose was added, and the samples were rotated at 4 °C for 1 h. After brief centrifugation, the supernatant was removed and samples were subjected to SDS/PAGE on 10% acrylamide gels.

Indirect Immunofluorescence. Cells grown on glass coverslips in 12-well plates were fixed in 2% paraformaldehyde for 10 min, then washed three times in PBS:glycine. Cells were permeabilized in 0.2% Triton X-100 for 10 min at 4 °C, then washed three times with immunofluorescence wash, and blocked with 10% goat serum for 1 h. Unconjugated primary antibodies were incubated in 10% goat serum for 2 h with gentle rocking, followed by three washes. Secondary antibodies conjugated to Alexa Fluor dyes (Invitrogen) were added for 1 h. Coverslips were then washed, incubated with DAPI for 5 min, and then mounted on glass slides with Prolong (Molecular Probes).

The 3D acinar structures grown in eight-well chamber slides were washed once in PBS, fixed in 5% formalin for 10 min, washed three times with PBS: glycine, permeabilized with 0.5% Triton X-100, washed three times with PBS: glycine, and then incubated in primary block (IF wash, 10% goat serum) for 1 h. Acini were incubated for 30 min in secondary block [IF wash, 10% goat serum, $F(ab')_2$]. Antibodies were diluted in secondary block and incubated for 2 h, followed by three washes with IF wash. Secondary antibodies were diluted in primary block and incubated for 1 h, followed by two IF washes and incubation with DAPI. Acini were mounted with Prolong. Tissue sections were processed for immunofluorescence as previously described (31). All fluorescence images were collected using an Axiovert 200M equipped with an Apotome imaging system. Images were analyzed using Axiovision software.

Proliferation Assay. Cells were seeded in 96-well plates (5,000 cells per well) and allowed to grow for the indicated lengths of time. The MTT (3-[4,5-dimethylthiazol-2-yl]-2,5 diphenyl tetrazolium bromide) Cell Proliferation Assay (ATCC) was used to monitor cell proliferation according to the manufacturer's suggested protocol.

Transwell Migration Assay. Cells were seeded in 24-well plates containing 8 μm transwell migration filters, then fixed and stained with DAPI, and the migrated cells quantified.

IP. Cells grown in 100 mm plates were lysed in a buffer composed of 50 mM Tris·HCl, 150 mM NaCl, 10 mM NaF, 0.7% CHAPS, and protease inhibitors. We incubated a 500 μg protein with 1 μg antibody and 25 μL Protein G Sepharose beads (GE Healthcare) at 4 °C for 2 h with rotation. The beads were washed twice in lysis buffer and the bound proteins eluted with sample buffer. The samples were subjected to SDS/PAGE on 10% acrylamide gels.

ACKNOWLEDGMENTS. We thank Drs. Nicholas Tonks, Linda Van Aelst, and Mahasin Osman as well as members of the S.K.M. and Tonks laboratories for helpful discussions. This work was supported by an American Cancer Society postdoctoral fellowship (PF-11-026-01-CSM, to M.E.F.) and National Cancer Institute Grant CA098830 (to S.K.M.).

1. Morris AJ, Malbon CC (1999) Physiological regulation of G protein-linked signaling. *Physiol Rev* 79(4):1373–1430.
2. Feigin ME (2013) Harnessing the genome for characterization of G-protein coupled receptors in cancer pathogenesis. *FEBS J* 280(19):4729–4738.
3. Lappano R, Maggiolini M (2011) G protein-coupled receptors: Novel targets for drug discovery in cancer. *Nat Rev Drug Discov* 10(1):47–60.
4. Dorsam RT, Gutkind JS (2007) G-protein-coupled receptors and cancer. *Nat Rev Cancer* 7(2):79–94.
5. O'Hayre M, et al. (2013) The emerging mutational landscape of G proteins and G-protein-coupled receptors in cancer. *Nat Rev Cancer* 13(6):412–424.
6. Prickett TD, et al. (2011) Exon capture analysis of G protein-coupled receptors identifies activating mutations in GRM3 in melanoma. *Nat Genet* 43(11):1119–1126.
7. Kan Z, et al. (2010) Diverse somatic mutation patterns and pathway alterations in human cancers. *Nature* 466(7308):869–873.
8. Liang H, et al. (2012) Whole-exome sequencing combined with functional genomics reveals novel candidate driver cancer genes in endometrial cancer. *Genome Res* 22(11):2120–2129.
9. Zhao Q, et al. (2010) Systematic detection of putative tumor suppressor genes through the combined use of exome and transcriptome sequencing. *Genome Biol* 11(11):R114.
10. Hammerman PS, et al.; Cancer Genome Atlas Research Network (2012) Comprehensive genomic characterization of squamous cell lung cancers. *Nature* 489(7417): 519–525.
11. Foulkes WD, Smith IE, Reis-Filho JS (2010) Triple-negative breast cancer. *N Engl J Med* 363(20):1938–1948.
12. Stevens KN, Vachon CM, Couch FJ (2013) Genetic susceptibility to triple-negative breast cancer. *Cancer Res* 73(7):2025–2030.
13. Matteson PG, et al. (2008) The orphan G protein-coupled receptor, Gpr161, encodes the vacuolated lens locus and controls neurulation and lens development. *Proc Natl Acad Sci USA* 105(6):2088–2093.
14. Leung T, et al. (2008) The orphan G protein-coupled receptor 161 is required for left-right patterning. *Dev Biol* 323(1):31–40.
15. Mukhopadhyay S, et al. (2013) The ciliary G-protein-coupled receptor Gpr161 negatively regulates the Sonic hedgehog pathway via cAMP signaling. *Cell* 152(1-2): 210–223.
16. Johannessen CM, et al. (2013) A melanocyte lineage program confers resistance to MAP kinase pathway inhibition. *Nature* 504(7478):138–142.
17. Debnath J, Muthuswamy SK, Brugge JS (2003) Morphogenesis and oncogenesis of MCF-10A mammary epithelial acini grown in three-dimensional basement membrane cultures. *Methods* 30(3):256–268.
18. Sancak Y, et al. (2007) PRAS40 is an insulin-regulated inhibitor of the mTORC1 protein kinase. *Mol Cell* 25(6):903–915.
19. White CD, Erdemir HH, Sacks DB (2012) IQGAP1 and its binding proteins control diverse biological functions. *Cell Signal* 24(4):826–834.
20. Alemayehu M, et al. (2013) β-Arrestin2 regulates lysophosphatidic acid-induced human breast tumor cell migration and invasion via Rap1 and IQGAP1. *PLoS ONE* 8(2): e56174.
21. Jadeski L, Mataraza JM, Jeong HW, Li Z, Sacks DB (2008) IQGAP1 stimulates proliferation and enhances tumorigenesis of human breast epithelial cells. *J Biol Chem* 283(2):1008–1017.
22. Noritake J, Watanabe T, Sato K, Wang S, Kaibuchi K (2005) IQGAP1: A key regulator of adhesion and migration. *J Cell Sci* 118(Pt 10):2085–2092.
23. Hayashi H, et al. (2010) Overexpression of IQGAP1 in advanced colorectal cancer correlates with poor prognosis-critical role in tumor invasion. *Int J Cancer* 126(11): 2563–2574.
24. Osman MA, Sarkar FH, Rodriguez-Boulan E (2013) A molecular rheostat at the interface of cancer and diabetes. *Biochim Biophys Acta* 1836(1):166–176.
25. Grohmanova K, et al. (2004) Phosphorylation of IQGAP1 modulates its binding to Cdc42, revealing a new type of rho-GTPase regulator. *J Biol Chem* 279(47):48495–48504.
26. Wang JB, Sonn R, Tekletsadik YK, Samorodnitsky D, Osman MA (2009) IQGAP1 regulates cell proliferation through a novel CDC42-mTOR pathway. *J Cell Sci* 122(Pt 12):2024–2033.
27. Tekletsadik YK, Sonn R, Osman MA (2012) A conserved role of IQGAP1 in regulating TOR complex 1. *J Cell Sci* 125(Pt 8):2041–2052.
28. White CD, Li Z, Dillon DA, Sacks DB (2011) IQGAP1 protein binds human epidermal growth factor receptor 2 (HER2) and modulates trastuzumab resistance. *J Biol Chem* 286(34):29734–29747.
29. Feigin M (2013) Harnessing the genome for characterization of G-protein coupled receptors in cancer pathogenesis. *FEBS J* 280(19):4729–4738.
30. Ory DS, Neugeboren BA, Mulligan RC (1996) A stable human-derived packaging cell line for production of high titer retrovirus/vesicular stomatitis virus G pseudotypes. *Proc Natl Acad Sci USA* 93(21):11400–11406.
31. Zhan L, et al. (2008) Deregulation of scribble promotes mammary tumorigenesis and reveals a role for cell polarity in carcinoma. *Cell* 135(5):865–878.